ORIGINAL RESEARCH

Daunorubicin-Loaded CdTe QDs Conjugated with Anti-CD123 mAbs: A Novel Delivery System for Myelodysplastic Syndromes Treatment

Dan Guo[1,2]
Peipei Xu[1]
Dangui Chen[1]
Lili Wang[1]
Yudi Zhu[1]
Yifan Zuo[1]
Bing Chen[1]

[1]Department of Hematology, Nanjing Drum Tower Hospital, The Affiliated Hospital of Nanjing University Medical School, Nanjing, Jiangsu 210093, People's Republic of China; [2]Department of Hematology, The Affiliated Hospital of Nantong University, Nantong, Jiangsu 226001, People's Republic of China

Introduction: The myelodysplastic syndromes (MDS) are a very heterogeneous group of myeloid disorders characterized by peripheral blood cytopenias and increase risk of transformation to acute myeloid leukemia (AML). Daunorubicin (DNR) is an indispensable drug for the treatment of MDS and AML. However, its side effects including cardiac toxicity and bone marrow suppression severely limit clinical application. Many researches reported high expression of CD123 antigen on high-risk MDS cells, so we constructed a novel drug delivery system comprising daunorubicin-loaded CdTe QDs conjugated with anti-CD123 mAbs (DNR-CdTe-CD123) to develop targeted combination chemotherapy for MDS.

Methods: CdTe conjugated antiCD123 through amide bond, co-loaded with DNR with electrostatic bonding. Then, we determined characterization and release rate of DNR-CdTe-CD123. The therapeutic effect and side effect of drug delivery system were evaluated through in vitro and in vivo experiments.

Results: CdTe showed appropriate diameter and good dispersibility and DNR was loaded into CdTes with high encapsulation efficiency and drug loading. The maximum drug loading and encapsulation efficiency were $42.08 \pm 0.64\%$ and $74.52 \pm 1.81\%$, respectively, at DNR concentration of 0.2mg/mL and anti-CD123 mAbs volume of 5ul (100ug/mL). Flow cytometry (FCM) showed that CD123 antigen was highly expressed on MUTZ-1 cells, and its expression rate was $72.89 \pm 10.67\%$. In vitro experiments showed that the inhibition rate and apoptosis rate of MUTZ-1 cells treated with DNR-CdTe-CD123 were higher than those in the other groups ($P<0.05$). Compared with the other groups, the level of apoptosis-related protein (P53, cleaved caspase-9, Bax and cleaved caspase-3) were upregulated in DNR-CdTe-CD123 group ($P<0.05$). In vivo experiments, DNR-CdTe-CD123 can effectively inhibit the tumor growth of MDS-bearing nude mice and reduce the side effects of DNR on myocardial cells.

Conclusion: The system of DNR-CdTe-CD123 enhances the therapeutic effects and reduce the side effects of DNR, thus providing a novel platform for MDS treatment.

Keywords: myelodysplastic syndrome, daunorubicin, CdTe, anti-CD123 monoclonal antibody, drug delivery system

Introduction

The myelodysplastic syndromes (MDS) are a heterogeneous group of myeloid disorders characterized by dysplastic and ineffective hematopoiesis.[1] The data from the NAACCR and SEER programs showed that MDS incidence rates reached 7.1–35.5 per 100 000 among patients aged 60 years and older, which indicates MDS is a common hematologic malignancy of the elderly.[2] With the development of population aging, the incidence of MDS may exceed that of leukemia and endanger

Correspondence: Bing Chen
Department of Hematology, Drum Tower Hospital, School of Medicine, Nanjing University, Nanjing, Jiangsu 210093, People's Republic of China
Email chenbing2004@126.com

people's health seriously. In addition, up to 30% of patients with MDS progress to acute leukemia.[3] Currently, the main treatment is chemotherapy in higher risk MDS besides hypomethylating agents. Daunorubicin (DNR), an anthracycline antibiotic, is one of the most effective chemotherapeutic agents for MDS and acute myeloid leukemia (AML).[4] However, its side effects including cardiac toxicity and bone marrow suppression severely limit clinical application.

Therefore, to overcome the limitations of the conventional chemotherapy, various drug delivery systems including liposomes, biological drug carriers, and nanocarriers have been developed in recent years.[5–8] Cadmium-tellurium (CdTe) quantum dot (QD) nanoparticles have received great attention due to their photostability and biocompatibility which are well suited for cancer diagnosis and therapy. Moreover, CdTe QDs have large-surface area for conjugating targeting ligands for targeted delivery.[9] In recent years, many scholars have used CdTe QDs as a drug delivery vehicle to construct drug-loaded nanosystem such as DNR-GA- Cys-CdTe NPs and DOX/GA-CdTe-CD22, which can deliver drugs to tumor cells, thereby improving the antitumor activity of the drug and attenuating its toxicity against normal tissues.[10,11]

CD123, an interleukin-3 receptor (IL-3R) alpha chain, is regarded as a marker of leukemia stem cells (LSCs) and is correlated with tumor load and poor prognosis.[12] Many reports have shown that CD123 is highly expressed on cells of high-grade MDS patients, similar to those in AML and it is low in normal hematopoietic stem cells and low-grade MDS.[13,14] Therefore, CD123 is an indicator for identifying malignant clonal cells in MDS and a candidate for targeted therapy.

At present, the treatment of MDS still lacks the target vector that can accurately transport anti-MDS drugs to tumor cells. In this study, a novel drug delivery system (DNR-CdTe-CD123) comprising anti-CD123-conjugated CdTe QDs co-loaded with DNR is synthesized to develop targeted combination chemotherapy for MDS. The system was characterized, and its antitumor effect and systematic toxicity were evaluated by in vitro and in vivo experiments. Additionally, the possible mechanism of their anti-tumor activity is depicted in Figure 1. This delivery system can precisely target MDS and facilitate preferential delivery of DNR into tumor cells which provides a new theoretical and experimental basis for MDS patients with targeted therapy.

Materials and Methods
Reagents and Animals

Daunorubicin hydrochloride (DNR·HCl) was obtained from Hisun Pharmaceutical Co., Ltd. (Zhejiang, China). EDC, sulfo-NHS and Dimethyl sulfoxide (DMSO) were purchased from Sigma–Aldrich (St Louis, USA). CdTe QDs were prepared as described elsewhere and used in our experiments.[15] Roswell Park Memorial Institute medium (RPMI) 1640 and Fetal bovine serum (FBS) were bought from Gibco Chemical Co. (Carlsbad, CA, USA). 4, 6-Diamidino-2-phenylindole (DAPI) staining solution was supplied by Beyotime Institute of Biotechnology (Shanghai, China). Pierce™ BCA Protein Assay Kit, Annexin V-Fluorescein isothiocyanate (FITC) apoptosis detection kit and hematoxylin–eosin kit were provided by KeyGen Biotech Co., Ltd. (Jiangsu, China). Cell counting kit-8 (CCK-8) assay was obtained from Dojindo Molecular Technologies, Inc. (Kyushu, Japan). Monoclonal antibodies for CD123, P53, Bax, cleaved caspase-3, cleaved caspase-9, and β-actin were from CST (MA, USA). All reagents used in this study were analytically pure.

The BALB/c-nude mice (four to six weeks, 18–22 g) were purchased from Shanghai National Center for Laboratory Animals (Shanghai, China) and maintained in specific pathogen-free (SPF) facilities with controlled temperature (23 ± 2°C) and humidity (60% ± 5%) and free access to food and water. The experimental procedures were based on the Guidelines for the Care and Use of Laboratory Animals (Chinese Council on Animal Research and the Guidelines of Animal Care) and all animals received humane care and their use was approved by the Animal and Ethics Review Committee of the Affiliated Drum Tower Hospital of Nanjing University Medical School (Nanjing, China).

Synthesis and Characterization of DNR-CdTe-CD123

The anti-CD123 mAbs were coupled to CdTe QDs using EDC/NHS methods.[16] Briefly, 0.2 mL of CdTe QDs (1mg/mL) and 0.1mL of EDC (1mg/mL) were incubated for 1 hr at room temperature in the dark. And 10ul anti-CD123 mAbs (1mg/mL) was incubated with 0.1mL of sulfo-NHS (1mg/mL) for 1 hr at room temperature in the dark. Then, carboxyl-activated CdTe was mixed with the amino-activated anti-CD123 for 1 hr under constant shaking of 100 rpm at 37°C. The anti-CD123-coupled CdTe QDs were purified after centrifugation at 13,000 rpm for 20 min.
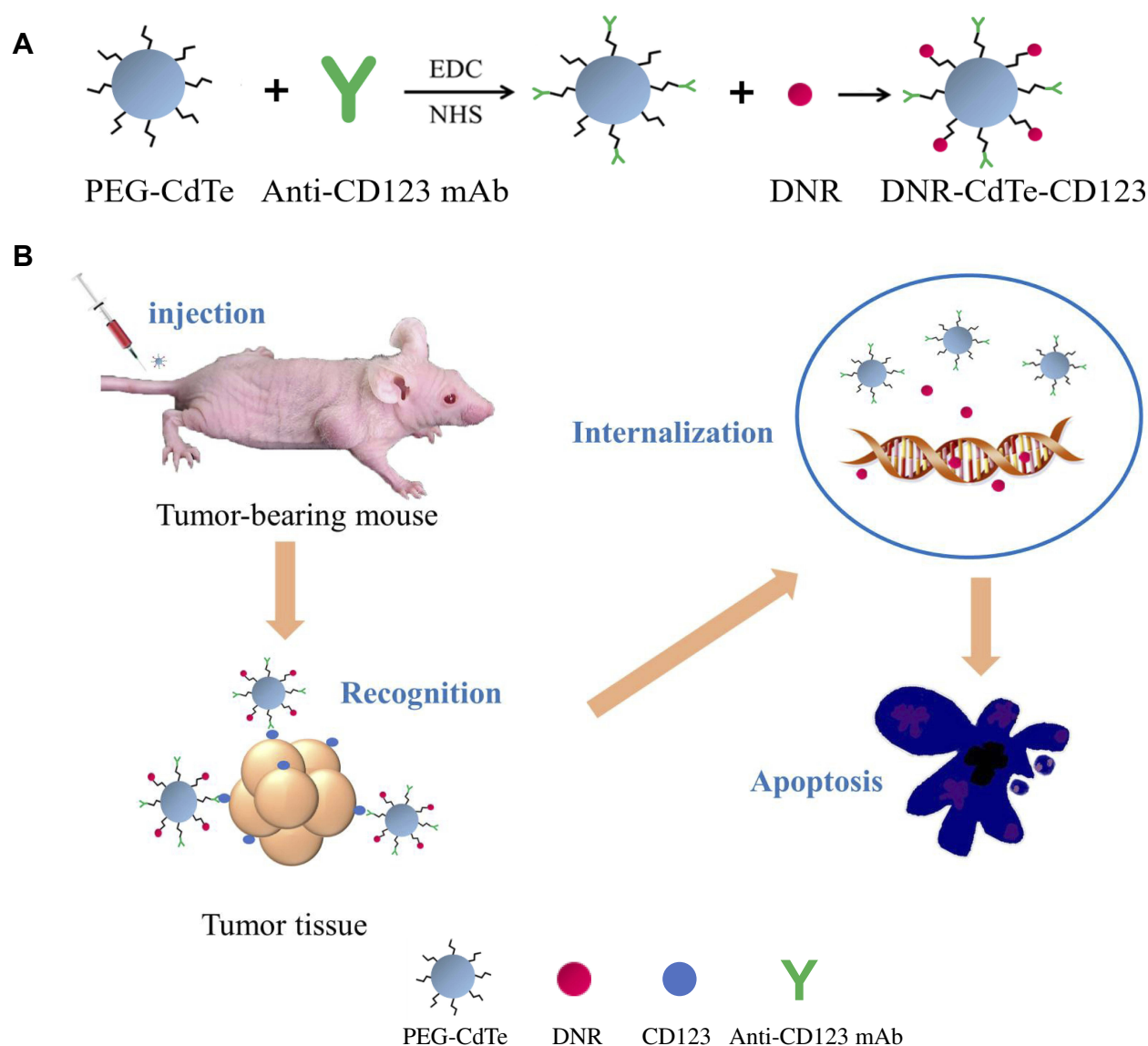
A

PEG-CdTe   Anti-CD123 mAb   DNR   DNR-CdTe-CD123

B

injection

Tumor-bearing mouse

Internalization

Recognition

Tumor tissue

Apoptosis

PEG-CdTe   DNR   CD123   Anti-CD123 mAb

Figure I Schematic of DNR-CdTe-CD123 preparation and mechanism of anti-tumor activity. (**A**) Schematic of DNR binding to PEG-CdTe QDs with the conjugation of anti-CD123 mAbs. (**B**) DNR-CdTe-CD123 can specifically target tumor cells by antigen-antibody binding and induce tumor cells apoptosis.

The DNR·HCl can efficiently be absorbed onto CdTe QDs through electrostatic interaction. 0.2 mL of DNR (1mg/mL) was added to the antiCD123-CdTe prepared above and then adding deionized water to 1mL under stirring for 22 h at 37°C in the dark. DNR-CdTe-CD123 was obtained after stepwise procedures involving centrifugation, discarding of the supernatant, washing, precipitation, and resuspension. Unbound DNR in the supernatant were determined by high-performance liquid chromatography (HPLC).

The morphological characteristics of the nanoparticles were observed under Transmission Electron Microscope (TEM). The dynamic light scattering (DLS) was used to measure hydrodynamic diameters, Zeta potential and size

distribution of QDs. Meanwhile, protein bands of CdTe, antiCD123-CdTe, and anti-CD123 mAbs were stained with Coomassie Brilliant Blue R250 following gel electrophoresis to determine whether the anti-CD123 mAbs were coupled to CdTe QDs. The drug-loading and encapsulation efficiencies were calculated as follows: Drug Loading (DL) = (Amount of drug in NPs/Amount of NPs) × 100%; Encapsulation Efficiency (EE) = (Amount of drug in NPs/Amount of the total drug) × 100%.

In vitro Release from DNR-CdTe-CD123

The release of DNR from DNR-CdTe-CD123 was measured at pH 6.0 (typical pH of the environment around the

tumor) and pH 7.4 (pH of physiological blood), respectively. 10 mL of DNR-CdTe-CD123 was enclosed in dialysis bags, which were then immersed in 200 mL phosphate-buffered saline (PBS) under continuous shaking (100 rpm) at 37°C. Aliquots (0.1 mL) were removed from the PBS at predetermined time intervals and an equivalent volume of fresh PBS was compensated. The DNR concentration was quantified by HPLC.

Cell Culture

MUTZ-1 cells, a cell line of MDS cells, were obtained from Shanghai Ze Ye Biological Technology Co., Ltd. (Shanghai, China). MUTZ-1 cells were grown in RPMI 1640 medium supplemented with 10% fetal bovine serum, 100 U/mL penicillin, and 100 μg/mL streptomycin in 5% CO2 and 95% air at 37°C in a humidified incubator. The cells undergo passage every 2–3 days to maintain the best state.

Imaging of MUTZ-1 Cells by Confocal Fluorescence Microscopy

MUTZ-1 cells (2×10^5/mL) were cultured in 5% CO2 at 37°C with DNR, DNR- CdTe, or DNR-CdTe-CD123 for 24 hrs. The cells were centrifuged, washed, and resuspended in PBS. Then, the obtained cell cultures were drop casted on a clean glass slide. The confocal fluorescence images of the samples were taken with a confocal inverted microscope after DAPI staining. The emission wavelengths of DAPI, FITC and DNR were 454, 525 and 592 nm, respectively. All the optical measurements were implemented at room temperature (25°C±2°C).

Cellular Uptake

Cellular uptake was quantitatively detected using flow cytometry (FCM) to determine if the intracellular concentration of DNR increased in DNR-CdTe-CD123-treated cells. Briefly, MUTZ-1 cells were incubated for 4 h with DNR, DNR-CdTe and DNR-CdTe-CD123. Then these cells were centrifuged and collected at 1000 rpm for 5 min. The culture medium was discarded and the precipitate was dispersed in 400 μL of PBS. Finally, the cellular uptake was analyzed via FCM. The relative fluorescence intensity of DNR was calculated as FI treated cells/FI control cells.

Cell Viability Assay

The CCK-8 assay was used to evaluate cell viability and the range of safe concentration of CdTe QDs. MUTZ-1 cells were seeded in a 96-well plate with 4×10^4 cells per well and treated with PBS (as the control group), anti-CD123, CdTe, DNR, DNR-CdTe and DNR-CdTe-CD123. The concentration of DNR was 2.0 μg/mL in different forms. Each group has three duplicates. After incubation for 24, 48, and 72 h at 37°C in a humidified atmosphere of 5% CO2, 10 μL of CCK-8 solution was added into each well and incubated for another 4 h. The optical density (OD) of the wells at 450 nm was read in a microplate reader. Growth inhibition rates (%) of MUTZ-1 cells were calculated as $(1-OD_{treatment}/OD_{control}) \times 100$. Different concentrations of CdTe QDs (0.05–0.8μg/mL) were added to MUTZ-1 cells or normal cells (PBMC), and the viability of cells was calculated in the same way. Every experiment was repeated at least three times.

Cell Apoptosis Study

MUTZ-1 cells (2×10^5/mL) were exposed to DNR, DNR-CdTe and DNR-CdTe-CD123 for 24 hrs. Afterwards, the cells were washed with cold PBS, followed by staining with 5 μL of Annexin V-FITC and 5 μL of propidium iodide (PI). FCM was used to quantitatively detect cell apoptosis. MUTZ-1 cells in different groups were also stained with DAPI and any morphological changes in the nuclei were observed under a fluorescent microscope.

Western Blot Analysis

MUTZ-1 cells were harvested after different treatments and subjected to Western blot analysis. Western blot was performed in accordance with standard protocols. Briefly, proteins of MUTZ-1 cells were extracted on ice using RIPA buffer (150 mM NaCl, 50 mM Tris-HCl pH 8, 0.5% sodium deoxycholate, 1% NP-40, 0.1% sodium dodecyl sulfate (SDS)). Total proteins (45 μg) were size fractionated by SDS/PAGE and transferred to a polyvinylidene difluoride membrane, then blocked for 1 h with 5% skimmed milk. Subsequently, the protein bands were incubated with monoclonal antibodies (P53, Bax, cleaved caspase-3 and cleaved caspase-9), and β-actin was used to normalize the data. The blots were detected by an enhanced chemiluminescence detection system.

Establishment of Tumor-Bearing Mouse Models

Nude mouse model of MDS xenografts Tumor-bearing mouse models were established by subcutaneously injecting 200 μL of MUTZ-1 cell suspension in PBS (5×10^7 cells/mL). The

tumor length and width were measured by a caliper and the tumor volume was calculated as follows: $V = 1/2 \times length \times (width)^2$. The tumor model was successfully established when the volume of tumor reached 80–150 mm^3.

In vivo Tumor Imaging

Tumor-bearing mice were randomly assigned into three groups: (1) DNR, (2) DNR-CdTe and (3) DNR-CdTe-CD123. Each mouse received 200 μL of the treatment agents (10 mg/kg DNR for the detection of its auto-fluorescence) via intravenous administration. The mice were anesthetized and imaged 24 h after injection by using an IVIS imaging system with the excitation wavelength of 485 nm and emission wavelength of 590 nm.

Tissue Distribution of DNR in Tumor-Bearing Mice

Tumor-bearing mice were intravenously administered with DNR, DNR-CdTe and DNR-CdTe-CD123 (DNR 5 mg/kg) with three mice in each group. The tumor tissues and main organs of mice were carefully isolated at 4 h after injection and then were washed, lysed and homogenized. DNR in the tissue homogenate was extracted by acidified isopropanol. After centrifugation, the supernatant was analyzed by spectrofluorometry (excitation wavelength: 485 nm, emission wavelength 590 nm).

Study of the Therapeutic Efficacy

The tumor-bearing mice were randomly divided into six groups with three mice in each group (a) PBS (control), (b) anti-CD123 mAbs, (c) CdTe, (d) DNR, (e) DNR-CdTe and (f) DNR-CdTe-CD123. Each mouse received 200 μL of the treatment agent every 3 days via tail vein and the equivalent dosage of DNR for a single dose was 3 mg/kg each. Tumor volume was measured 0, 2, 4, 6, 8, 10, and 12 days after the treatment. The relative tumor volume (RTV) was calculated as follows: RTV=V/V0 (V0 represents the initial tumor volume before treatment). After 12 days, the serum concentrations of alanine transaminase (ALT), creatinine (Cr), urea nitrogen (BUN) and creatine kinase-MB (CK-MB) were detected to evaluate hepatic function, renal function and myocardial injury. Then, all the mice were sacrificed and the tumor, heart, liver, spleen, lung and kidney were removed for further experiments.

Histopathological Examination

The tumor tissues and major organs of mice were isolated carefully, washed by PBS and then fixed in 4% formaldehyde solution at 4°C overnight. Afterwards, they were embedded in paraffin blocks, sectioned and stained with hematoxylin–eosin for histopathological examination.

Immunofluorescence Assay

Frozen sections of tumors were prepared and washed with PBS until room temperature was reached. The sections were blocked with 5% BSA supplemented with 0.3% Triton-X 100 for 1 h, then added with diluted primary antibodies (P53, Bax, cleaved caspase-3 and cleaved caspase-9). The sections were incubated at 37°C for 1 h in a wet box and IgG–FITC, as secondary antibody, was incubated for 1 h at room temperature in the dark. After the cell nuclei were stained by DAPI, the sections were covered with antifade mounting medium and observed under a fluorescent microscope.

Statistical Analysis

The data were expressed as the means ± standard deviation. Statistical analyses were performed with Student's t-test using the SPSS software (Version 22.0; Chicago, US). The value $P<0.05$ was considered statistically significant.

Results
Characterization of DNR-CdTe-CD123

The PEG-modified CdTe QDs were visually characterized by transmission electron microscopy (TEM). As Figure 2A showed, the CdTe QDs had relatively uniform dispersed particles and good crystal structure, and the average particle size was about 7 nm. The results of Coomassie Brilliant blue staining (Figure 2B) indicated that anti-CD123 mAbs were successfully linked to CdTe QDs and the ligation rate was about 70%. The particle size distribution was determined by dynamic light scattering experiments. The average hydrodynamic diameter of CdTe QDs 7.13 nm, and the average hydrodynamic size of DNR-CdTe-CD123 is 114.91 nm (Figure 2C and D). The zeta potential demonstrates that after attachment of DNR and anti-CD123 mAbs to the surface of the CdTe QDs, the relevant zeta potential value changed from −12.5 ± 1.57 to −32.93 ± 1.0 mV (Figure 2D).

The high surface-volume ratio of CdTe QDs makes it easy to load them with a great amount of DNR. The drug loading (DL) and encapsulation efficiency (EE) were
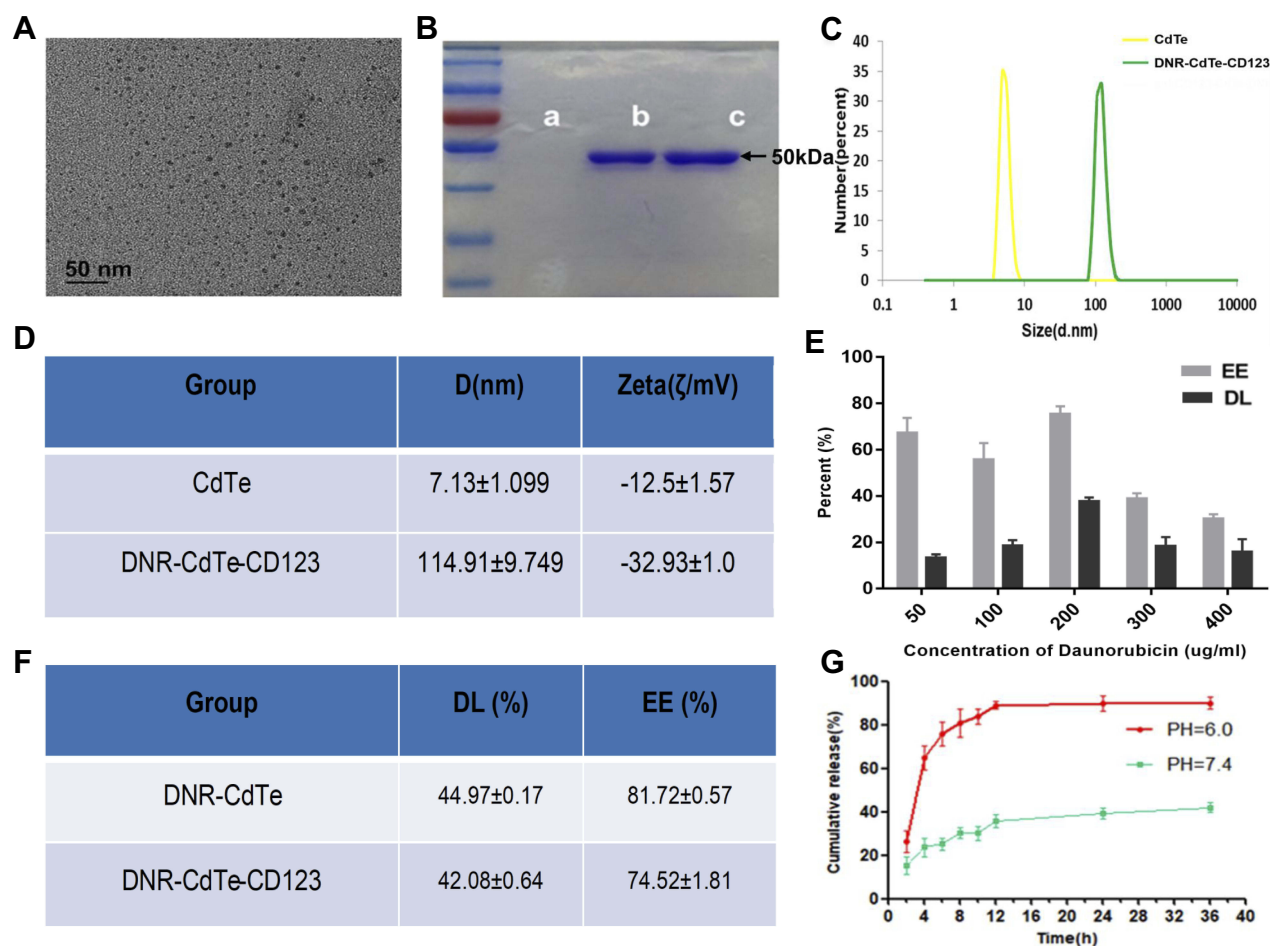
Figure 2 Characterization of DNR-CdTe-CD123. (**A**) TEM image of PEG-CdTe. (**B**) Protein bands of PEG-CdTe (a), antiCD123-CdTe (b) and anti-CD123 mAbs (c) stained by Coomassie Brilliant blue R250. (**C**) DLS analysis of CdTe and DNR-CdTe-CD123. (**D**) The sizes and zeta potential of CdTe and DNR-CdTe-CD123. (**E**) Encapsulation efficiency and drug loading of DNR-CdTe with different concentration of DNR. (**F**) The maximum encapsulation efficiency and drug loading of DNR-CdTe and DNR-CdTe-CD123. (**G**) Cumulative in vitro DNR release behaviors at pH 6.0 and 7.4.

measured by high-performance liquid chromatography. When the concentration of DNR was 0.2mg/mL, the drug loading rate and encapsulation efficiency of DNR-CdTe reached the maximum value ($44.97 \pm 0.17\%$; $81.72 \pm 0.57\%$). The maximum DL and EE were $42.08 \pm 0.64\%$ and $74.52 \pm 1.81\%$, respectively, at anti-CD123 mAbs volume of 5ul (100ug/mL) (Figure 2E and F).

The cumulative release of DNR from DNR-CdTe-CD123 was performed in the PBS with different pH values (Figure 2G). The most rapid release of DNR was obtained at pH=6.0 and approximately 90% of the loaded DNR was released into the buffer within 24 hrs. However, the release rate of DNR at pH 7.4 was considerably slow, and only 40% of the DNR was released within 24 hrs, which suggested the release of DNR from DNR-CdTe-CD123 was pH-triggered. Because the tumor tissues were with acidic microenvironment, an efficient DNR release and accumulation can be obtained in the target tumor tissues.

Cytotoxic Effects of DNR-CdTe-CD123 in vitro

MUTZ-1 cells are a line of MDS cell. Flow cytometry (FCM) showed that CD123 antigen was highly expressed on MUTZ-1 cells, and its expression rate was $72.89 \pm 10.67\%$ (Figure 3A). The fluorescence images under a laser scanning confocal microscope further confirmed that DNR and anti-CD123 mAbs were conjugated to the CdTe QDs (Figure 3B). Moreover, DNR markedly accumulated in MUTZ-1 cells in the DNR-CdTe-CD123 group compared with that in DNR alone and DNR-CdTe group. Thus, anti-CD123-conjugated CdTe QDs could enhance intracellular drugs concentration through actively targeting tumor cells. Prior to in vitro and vivo application, the cytotoxicity of CdTe QDs was tested by CCK-8 assay. As Figure 4A showed, the viability of MUTZ-1 cells and normal cells was not inhibited significantly when the concentration of CdTe was 0.05–0.8ug/mL ($P>0.05$). In order
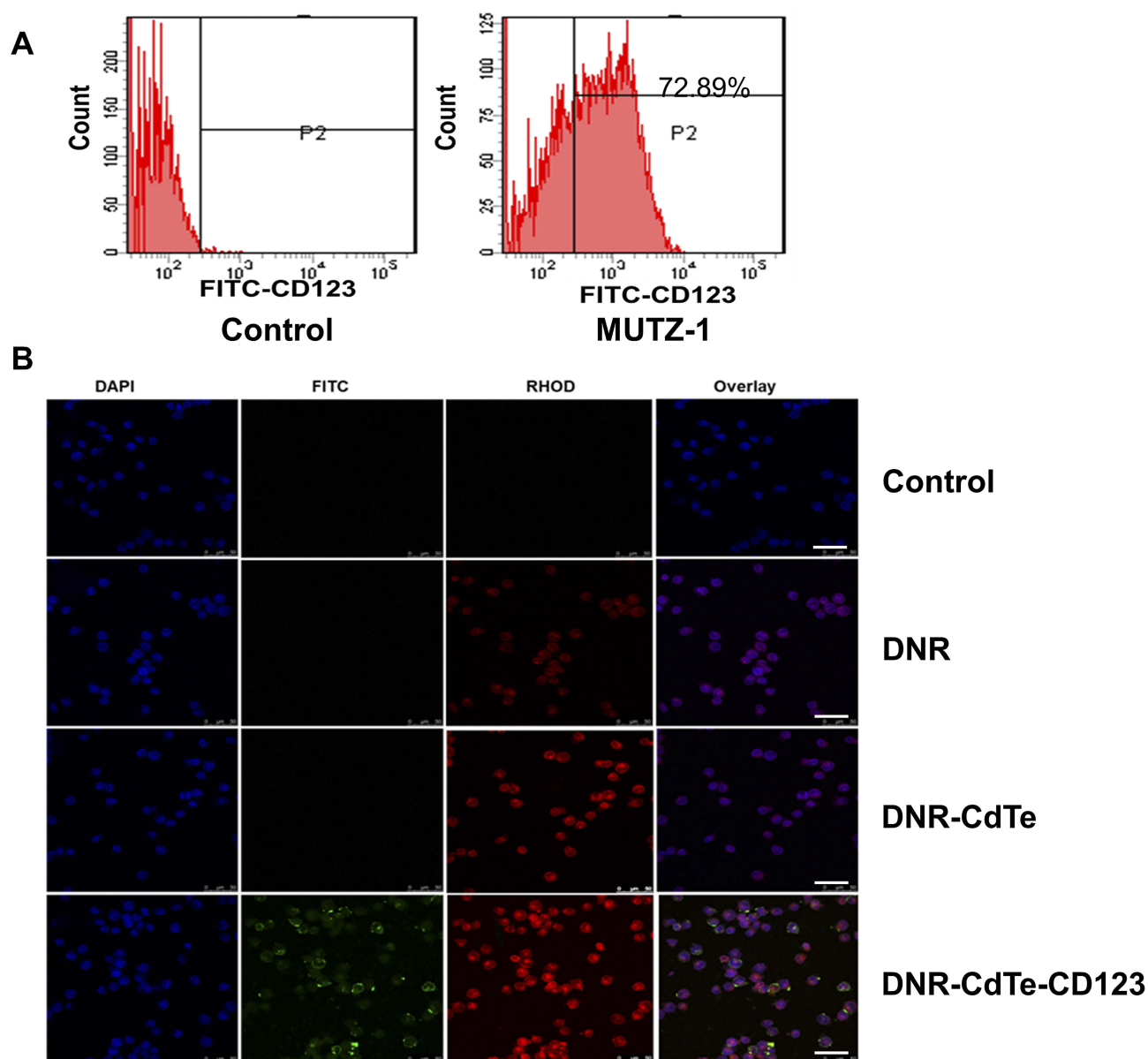
Figure 3 (**A**) Detection of CD123 antigen on MUTZ-1 cells by flow cytometry. (**B**) Confocal microscopy images of MUTZ-1 cells, respectively, treated with PBS (control), DNR, DNR-CdTe and DNR-CdTe-CD123 after DAPI staining (scale bar: 20 μm, ×200). Anti-CD123 mAbs were cross-linked with FITC and DNR autofluorescence is red.

to detect cells viability after different treatment, MUTZ-1 cells were treated with DNR, DNR-CdTe and DNR-CdTe-CD123 in different concentrations of DNR (0.25, 0.5, 1.0, 2.0 and 4.0 μg/mL), and the cytotoxic effects were evaluated using CCK-8 assay. The IC50 values for DNR, DNR-CdTe and DNR-CdTe-CD123 were 2.33 μg/mL, 1.76 μg/mL, and 0.89 μg/mL, respectively (Figure 4B). As illustrated in Figure 4C, the inhibition rates in MUTZ-1 cells treated with DNR-CdTe-CD123 were 76%, 84% and 93% after incubation for 24, 48 and 72 h, which were higher than those determined in the other groups ($P<0.05$).

Additionally, the growth inhibition rates of normal cells (PBMC) that were treated with free DNR were significantly higher than that of cells treated with DNR-CdTe or DNR-CdTe-CD123 ($P<0.05$) (Figure 4D). Therefore, CdTe QDs conjugated with anti-CD123 mAbs could enhance drug cytotoxicity through targeted delivery.

Cellular Uptake and Apoptosis

To determine if the CdTe QDs that were conjugated with anti-CD123 mAbs can exclusively facilitate DNR accumulation in CD123+ tumor cells, drug concentration in
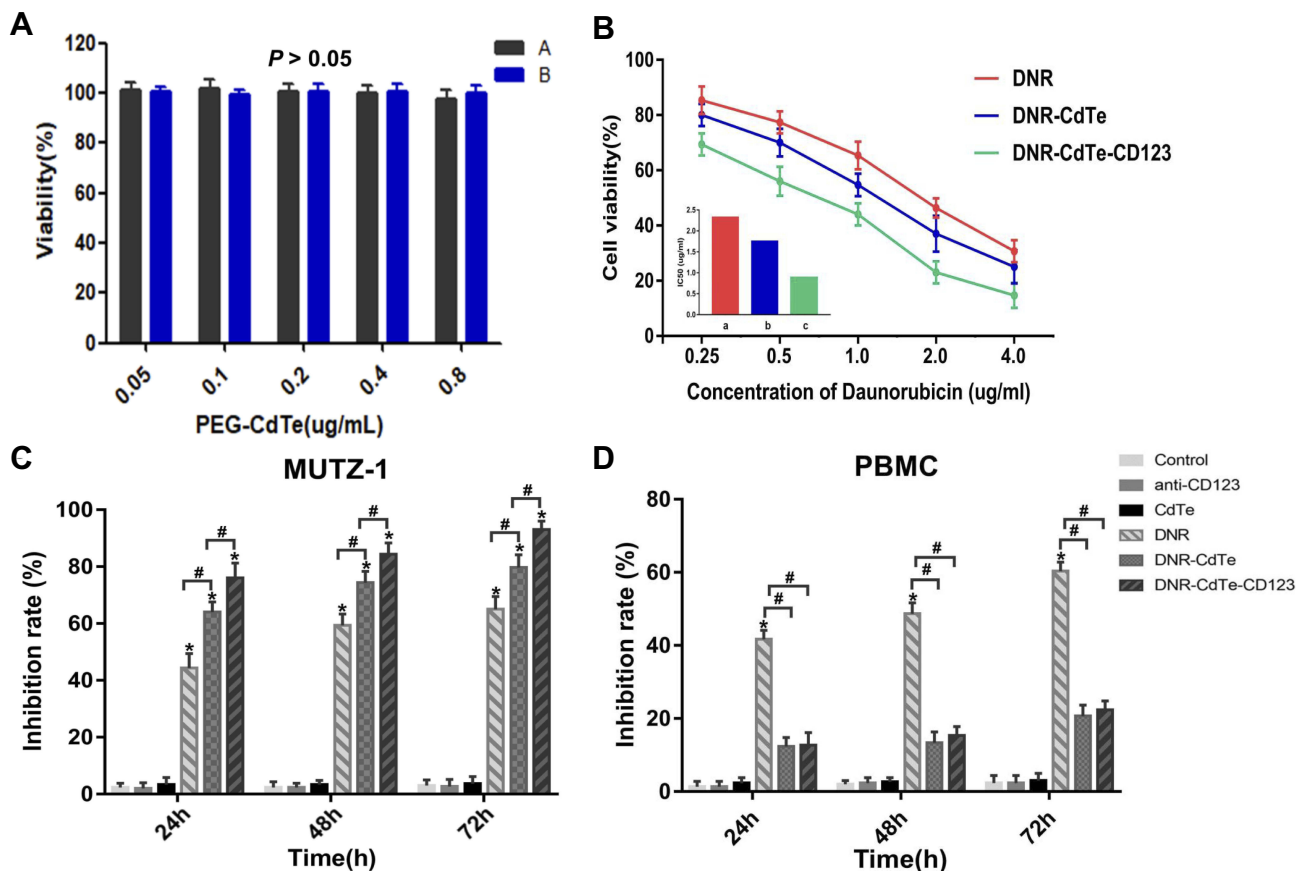
Figure 4 Cytotoxic effects of DNR-CdTe-CD123 against MUTZ-1 cells. (**A**) The cytotoxicity of PEG-CdTe tested by CCK-8 assay ($P>0.05$). (**B**) The cytotoxic effects of DNR, DNR-CdTe and DNR-CdTe-CD123 against MUTZ-1 cells with different concentration of DNR; Inset: The IC50 of DNR in different groups for MUTZ-1 cells at 24 hrs. a: DNR; b: DNR-CdTe; c: DNR-CdTe-CD123. (**C** and **D**) Growth inhibition of MUTZ-1 and PBMC cells treated with PBS, anti-CD123, CdTe, DNR, DNR-CdTe and DNR-CdTe-CD123 at 24, 48 and 72 hrs. (*$P<0.05$ when compared with controls, #$P<0.05$).

MUTZ-1 cells was determined by FCM analysis of intracellular fluorescence intensity. As shown in Figure 5A, intracellular DNR concentration significantly increased in MUTZ-1 cells that were treated with DNR-CdTe-CD123 compared with those in cells treated with DNR alone or DNR-CdTe. This result positively correlated with the cytotoxic activity. FCM was also used to quantitatively investigate the apoptosis of MUTZ-1 cells (Figure 5B and C). After the incubation for 24 h, the total apoptosis percentages were 5.06%, 5.56%, 6.3%,30.4%, 62.06%, and 76.9% in untreated cells, cells treated with anti-CD123 mAbs, CdTe, DNR, DNR-CdTe and DNR-CdTe-CD123, respectively. Apoptosis levels among cells that were treated with DNR, DNR-CdTe and DNR-CdTe-CD123 were significantly different and the highest rate of apoptosis was observed in the DNR-CdTe-CD123 group ($P<0.05$). Fluorescence microscopy was used to observe the morphological changes in MUTZ-1 cells stained with DAPI. Chromatin stained homogeneously in untreated cells, as shown in Figure 6. When

MUTZ-1 cells were treated with DNR, an apoptotic appearance, which was characterized by chromatin condensation, nucleolus pyknosis, and nuclear fragmentation, was observed in these cells. The morphological changes were particularly pronounced when the DNR-CdTe-CD123 was used against the MUTZ-1 cells, thus demonstrating that DNR-CdTe-CD123 improved the ability of DNR to induce cell apoptosis.

Western Blot Analysis

To further understand the antitumor mechanism of DNR-CdTe-CD123, Western blot assay was performed to analyze the expression levels of P53, cleaved caspase-9, Bax and cleaved caspase-3 in MUTZ-1 cells treated with different agents. Compared with the controls, the protein expression levels of P53, cleaved caspase-9, Bax and cleaved caspase-3 were upregulated in cells that were treated with DNR, DNR-CdTe and DNR-CdTe-CD123 (Figure 7A and B). Moreover, these changes were
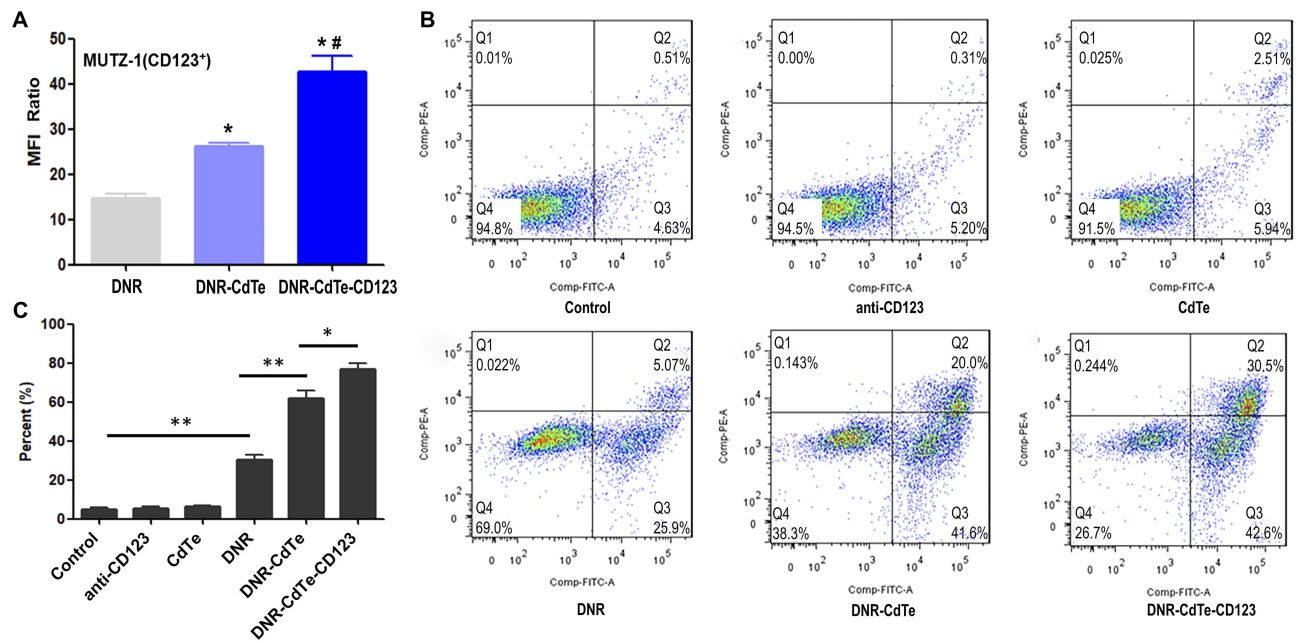
Figure 5 Mean fluorescence intensity (MFI) in MUTZ-1 cells and apoptosis of MUTZ-1 cells. (**A**) FCM was utilized to determine the uptake of DNR by MUTZ-1 cells. The bar graph shows comparative intracellular DNR uptake in different groups, as quantified by MFI. (*$P<0.05$ when compared with DNR, #$P<0.05$ when compared with DNR-CdTe). (**B**) The apoptosis of MUTZ-1 cells with different treatments was detected using FCM. (**C**) Quantitative data of apoptosis from (**B**) (*$P<0.05$, **$P<0.01$).
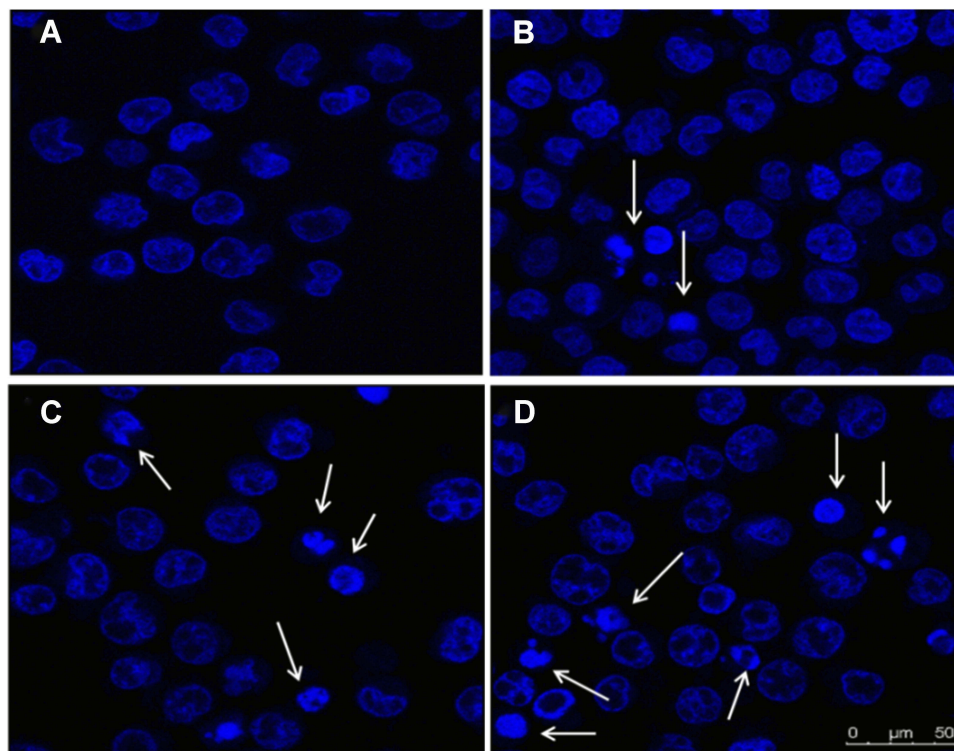
Figure 6 The fluorescence microscopy images of MUTZ-1 cells after DAPI staining (scale bar: 50 μm). (**A**) Control; (**B**) DNR; (**C**) CdTe-DNR; (**D**) DNR-CdTe-CD123. Cell apoptosis is indicated by arrows.

A

B
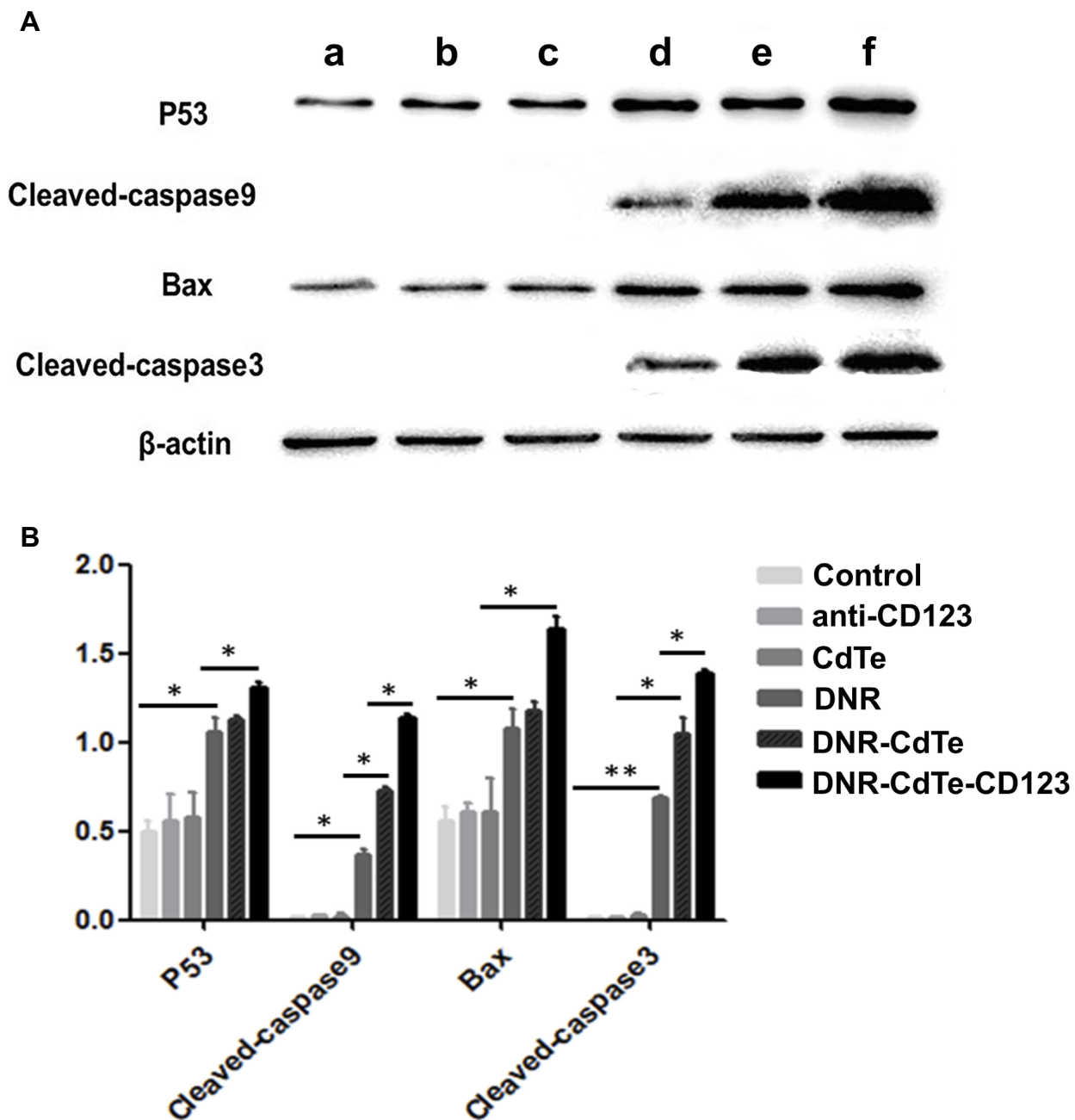
Figure 7 (**A**) Western blot analysis of apoptosis-related proteins expression levels.a, Control; b, anti-CD123; c, CdTe; d, DNR; e, DNR-CdTe; f, DNR-CdTe-CD123. (**B**) Quantified analysis of Western blot gray values. (*P<0.05, **P<0.01).

particularly significant in the DNR-CdTe-CD123 group (P<0.05). These results confirmed that DNR-CdTe-CD123 exhibited the highest antitumor activity among the others.

Anti-Tumor Activity of DNR-CdTe-CD123 in vivo

The distribution of DNR in tumor-bearing mice was visualized using vivo imaging system 24 h after the treatment.

Figure 8A shows that DNR fluorescence intensity in tumor sites of DNR-CdTe-CD123-treated mice obviously increased, which was significantly higher than that in DNR- and DNR-CdTe-treated mice. The findings revealed that loading DNR on CdTe QDs conjugated with anti-CD123 mAbs greatly improved DNR accumulation in tumor tissues.

Next, the results of tissue distribution are shown in Figure 8B. The mice treated with DNR had a low drug
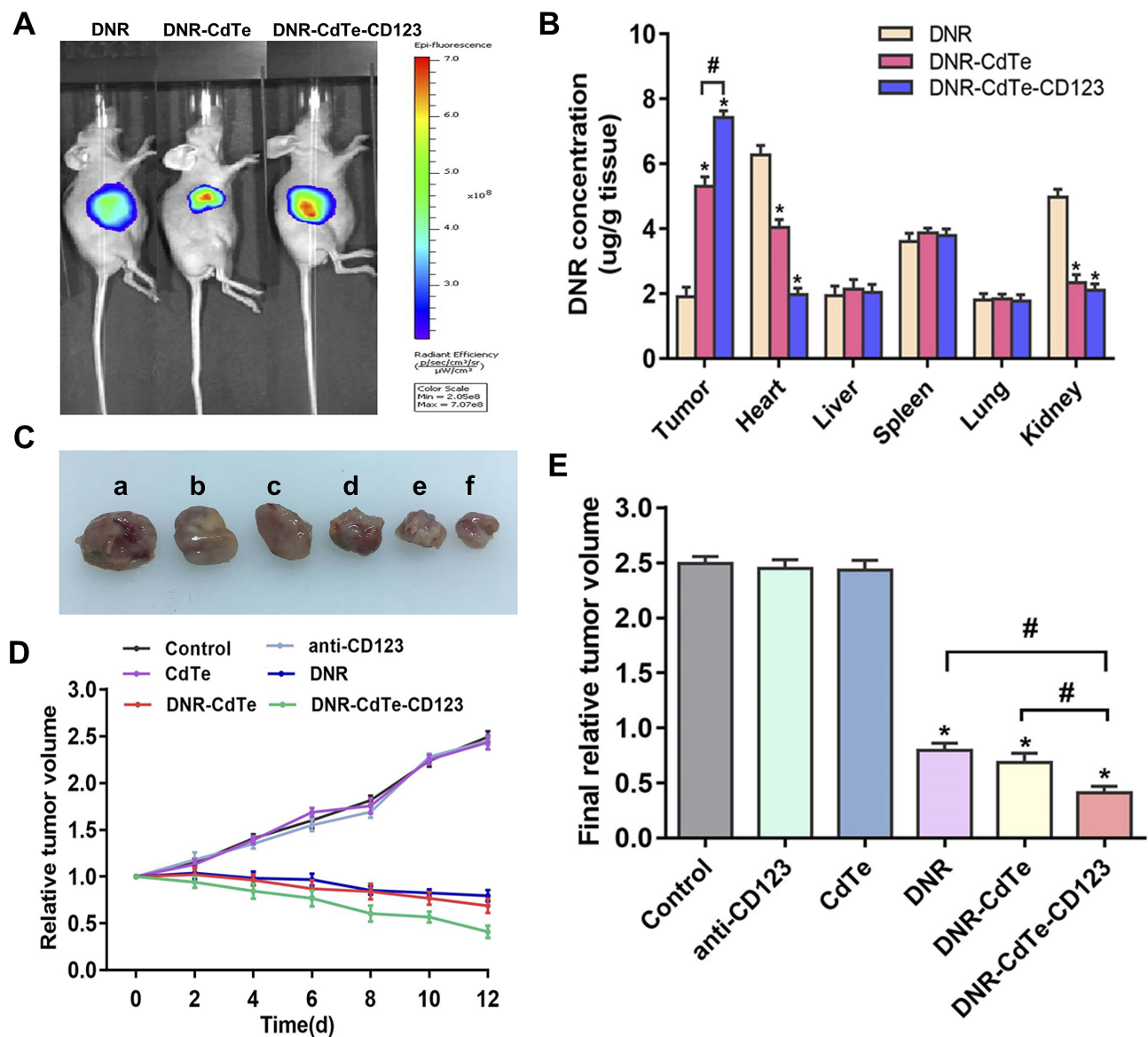
Figure 8 Effects of DNR-CdTe-CD123 in vivo. (**A**) Fluorescence images of tumor-bearing mice treated with DNR, DNR-CdTe and DNR-CdTe-CD123. (**B**) Tissue distribution of DNR at 4 hrs after injection with DNR, DNR-CdTe or DNR-CdTe-CD123. (**C**) Isolated tumor bodies. a, control; b, anti-CD123; c, CdTe; d, DNR; e, DNR-CdTe; f, DNR-CdTe-CD123. (**D**) The changes in relative tumor volume of mice in the period of 12 days with different treatments. (**E**) The final relative tumor size of mice in different groups. (*$P<0.05$ when compared with control, #$P<0.05$).

concentration in tumor tissues and a high one in heart tissues. In contrast, the heart tissues in the DNR-CdTe-CD123-treated mice had a significantly lower concentration of DNR than that in the mice treated with DNR ($P<0.05$). And the tumor tissues of mice treated with DNR-CdTe-CD123 had higher concentration of DNR than that with DNR ($P<0.05$).

To investigate the therapeutic effects of DNR-CdTe-CD123 in vivo, the tumor size of mice was measured every 2 days. The tumor volume of mice in the control, anti-CD123 mAbs and CdTe group increased continuously,

whereas the tumor volume was decreased over time after treatment in the DNR, DNR-CdTe and DNR-CdTe-CD123 groups (Figure 8C and D). The smallest tumor volume was observed in the DNR-CdTe-CD123 group at the end of the experiments, which was significantly smaller than those from the other groups ($P<0.05$) (Figure 8E). The sheet necrosis of tumor tissues was observed in the DNR, DNR-CdTe and DNR-CdTe-CD123 groups by hematoxylin-eosin (H&E) staining and the results showed that apoptosis in tumor tissues from mice that were treated with DNR-CdTe-CD123 obviously increased (Figure 9).
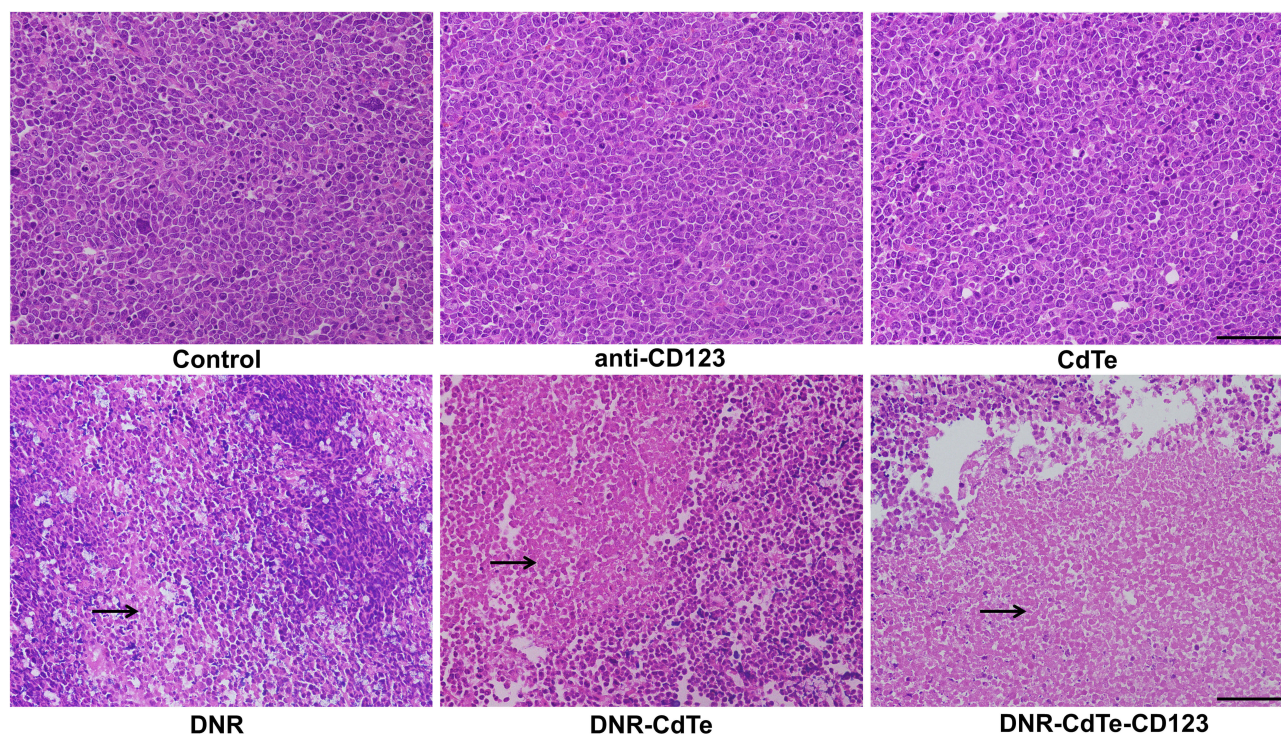
Figure 9 Histopathological examination of tumor tissues in tumor-bearing mice on day 12 after treatment (hematoxylin-eosin staining, ×40). The sheet necrosis of tumor tissues is indicated by arrows.

Toxicity of DNR-CdTe-CD123 Towards Normal Tissues

The serum concentrations of alanine transaminase (ALT), creatinine (Cr), blood urea nitrogen (BUN) and creatine kinase-MB (CK-MB) of mice were detected on day 12 after treatment. Figure 10A shows that only the CK-MB concentration in the DNR group was significantly different from that in the control group ($P<0.05$). The histopathological changes on major organs of tumor-bearing mice were conducted by H&E staining after different treatments and are shown in Figure 10B. No apparent pathological changes were observed in the heart, liver, spleen, lung and kidney of mice except those treated with free DNR. Typical DNR-induced myocardial injury was observed in the DNR treated mice. Therefore, DNR delivered by CdTe and anti-CD123 mAbs can protect the heart from the direct exposure to DNR.

During the treatment, the body weight was also monitored every two days. As shown in Figure 10C and D, the body weight of mice in the groups treated with normal saline, anti-CD123 mAbs, CdTe, DNR-CdTe and DNR-CdTe-CD123 increased obviously compared with the initial body weight. However, after the treatment with free DNR for 12 days, the mice had a final average weight

of 17.77 g, indicating a remarkable weight loss compared with the other groups. This finding revealed that the toxicity of DNR against normal tissue was serious and was reduced by the encapsulation of CdTe QDs.

Apoptosis Mechanisms of DNR-CdTe-CD123 Antitumor Effects in vivo

Tumors were harvested from mice after treatment and immunofluorescence staining was performed to better understand the mechanism by which DNR-CdTe-CD123 inhibits tumors. The green fluorescence intensity of P53, cleaved caspase-9, Bax and cleaved caspase-3 gradually increased in the tumor tissues of mice in the DNR alone, DNR-CdTe and DNR-CdTe-CD123, as shown in Figure 11. The results exhibited the same trends as the Western blot data that were obtained from MUTZ-1 cells in vitro. Therefore, the genes that encode P53, Bax, caspase-9 and caspase-3 were related to the antitumor activity of DNR.

Discussion

MDSs comprise bone marrow stem cell disorders characterized by peripheral blood cytopenias and increased risk of transformation to acute myelogenous leukemia (AML).[17] So far, there is no pharmacologic treatment to
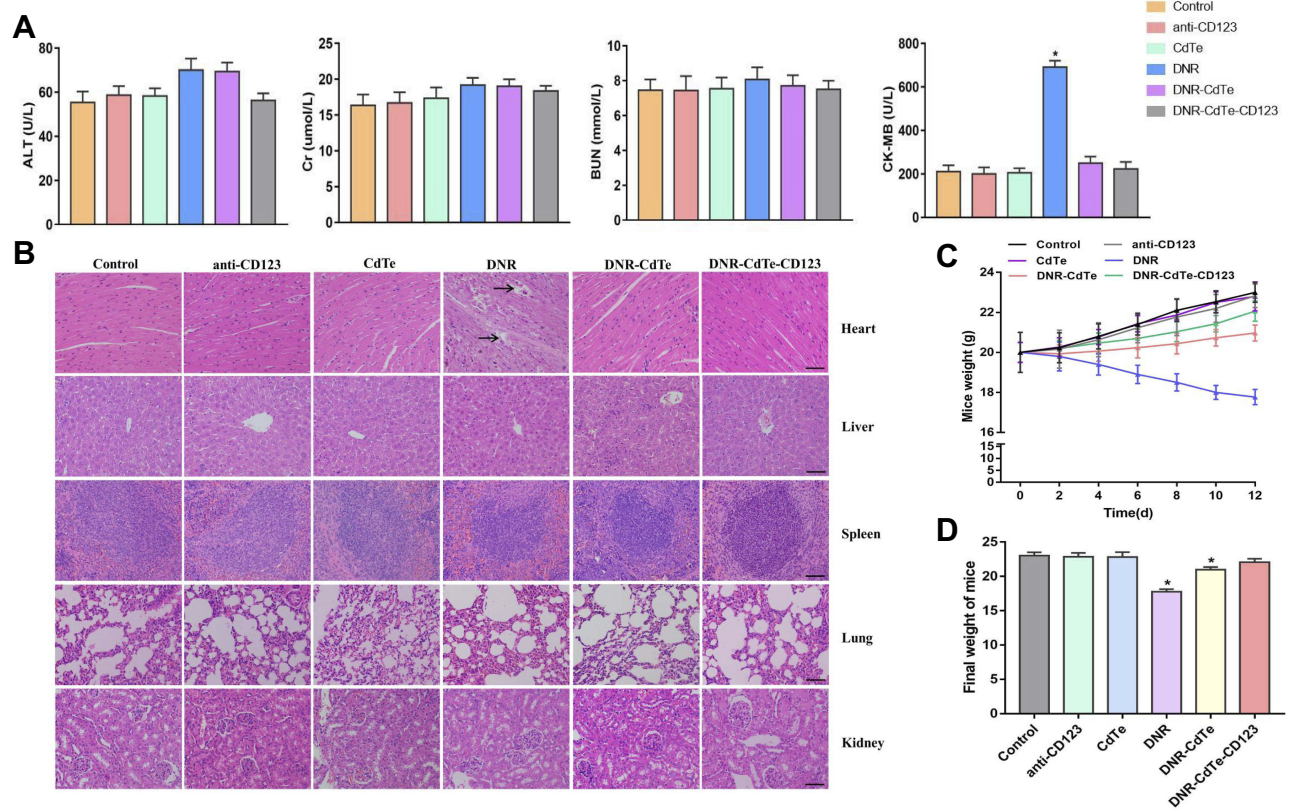
Figure 10 Toxicity on normal tissues of mice in different groups. (**A**) Serum concentration of ALT, Cr, BUN and CK-MB were detected at day 12 posttreatment. (**B**) Hematoxylin-eosin staining of heart, liver, spleen, lung and kidney tissues from mice after different treatments (scale bar: 200μm; ×40). Histopathological changes are indicated by arrows. (**C**) The body weight changes of mice in the period of 12 days after different treatments. (**D**) The final body weight of mice in different groups. (*$P<0.05$ when compared to control).
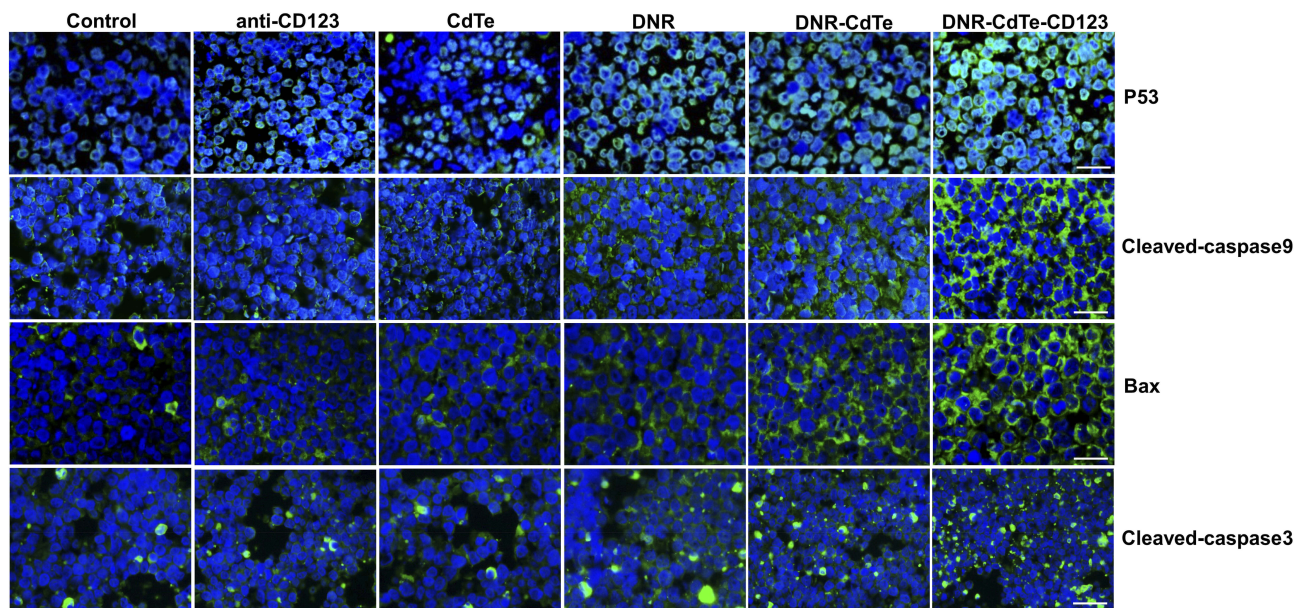

Figure 11 Immunofluorescence images of tumor sections from mice with different treatments (scale bar: 10μm, ×200). The cell nuclei were stained with DAPI and the secondary antibodies were cross-linked with FITC against primary antibodies for P53, cleaved caspase-9, Bax and cleaved caspase-3.

cure the disease. Allogeneic stem cell transplantation (ASCT) represents the option with a potential cure rate of 30% to 50% in MDS.[18] However, therapeutic options are limited in patients unsuitable for ASCT. AML-like protocols in higher risk MDS have generally used classical anthracycline-araC combinations.[19] As an anthracycline antibiotic, DNR inhibit proliferation and induce apoptosis of tumor cells by damaging DNA.[20] However, the dose-related anthracycline toxicity, especially cardiotoxicity, might limit further treatment intensification.[21] Moreover, MDS occurs more frequently in older patients and they often present with significant cardiac comorbidity rendering the use of nontargeted anthracyclines hazardous.

Many researchers reported that CD123 is highly expressed in cells of high-risk MDS but is low in normal stem cells.[13,22,23] Therefore, the CD123 molecule has better tumor specificity for MDS and anti-CD123 mAbs conjugated with drug can be rapidly internalized into MDS cells, resulting in intracellular delivery of the drug. In this work, the delivery system of DNR-CdTe-CD123 were fabricated with the aim to target MDS cells and precisely deliver loaded DNR to tumor cells for targeted chemotherapy. As a drug carrier, polyethylene glycol-modified CdTe QDs have good hydrophilicity and biocompatibility. And our study indicated that DNR-CdTe-CD123 possessed high EE and DL of the drugs. The particle diameter of DNR-CdTe-CD123 (114.91 nm) was optimal in vivo delivery (Figure 2C), as the particles with size more than 10 nm could escape rapid renal clearance and the sizes more than 200 nm could be preferentially phagocytized by the reticuloendothelial system of the spleen and liver.[24] As shown in Figure 2E, the drug release of DNR was pH sensitive and more DNR was released at low pH. So most of the loaded DNR would be released in the tumor tissues because of the acidic microenvironment around in the tumor tissue and inside the subcellular organelle.

The in vitro anti-tumor effects of DNR -CdTe-CD123 were subsequently evaluated. The increased intracellular DNR concentration indicated that delivery with CdTe and anti-CD123 mAbs increased DNR uptake by MUTZ-1 cells. A tumor-bearing mouse model was established to estimate the in vivo effects of DNR -CdTe-CD123. The tumor volumes of DNR, DNR-CdTe and DNR-CdTe-CD123 mice significantly decreased compared with those of the controls. Moreover, the tumor size was the smallest in the DNR-CdTe-CD123 group and the apoptosis of tumor tissues was most pronounced in the DNR-CdTe-CD123 group. This finding illustrates that DNR-CdTe-CD123 remarkably improves the efficacy of DNR in MDS treatment.

However, what should be noted is nano-safety and nanotoxicity. In our study, as another control group, the CdTe group showed that there was safe and low cytotoxic at a low concentration. Dose-dependent cardiotoxicity of DNR critically limits its clinical use. Our results showed that DNR-CdTe-CD123 caused no significant functional and pathological changes in major organs such as heart, liver, spleen, lung and kidney and cardiac toxicity occurred only upon treatment with free DNR, as evident by the elevated CK-MB and myocardial pathological damage (Figure 10A and B). As a clinical symptom, weight loss is an early indicator of side effects. In our study, weight loss was found only in the group receiving free DNR treatment. This result further confirmed that when CdTe act as drug carriers, the therapeutic efficacy of DNR is improved and side effects are reduced.

Apoptosis, a cell death program, is regulated by intrinsic and extrinsic pathways. The intrinsic pathway responds to signals such as DNA damage and activates "executioner" caspases through a mitochondria-dependent pathway and the extrinsic pathway is activated by the binding of ligands to corresponding death receptors.[25] P53 is a major player in the apoptotic response of cells and regulates the expression of some downstream apoptosis genes, such as Bax and Bcl-2.[26] Bax is a pro-apoptotic gene in Bcl-2 family members.[27] Bax can improve the permeabilization of the mitochondrial outer membrane, subsequently activating downstream caspase-9 and the final stage of apoptosis occurs once caspase-9 initiates the cleavage of procaspase-3.[28] Our data revealed the increased protein expression levels of P53, Bax, cleaved caspase-9, and cleaved caspase-3 after the DNR treatment both in vitro and in vivo. This increment was more obvious in the DNR-CdTe-CD123 group which revealed that the pro-apoptotic pathway promotes the apoptosis by intrinsic pathway.

In this study, we constructed a DNR-CdTe-CD123 targeting carrier system successfully with high drug loading efficiency and entrapment efficiency. DNR-CdTe-CD123 can proactively target CD123 antigen on the surface of MUTZ-1 cells, which can effectively transport DNR to tumor cells. The system enhances the therapeutic effects and reduces the side effects of DNR, thus providing a novel platform for MDS treatment.

Acknowledgments

References

1. Troy JD, Atallah E, Geyer JT, Saber W. Myelodysplastic syndromes in the United States: an update for clinicians. *Ann Med*. 2014;46 (5):283–289. doi:10.3109/07853890.2014.898863

2. Rollison DE, Howlader N, Smith MT, et al. Epidemiology of myelodysplastic syndromes and chronic myeloproliferative disorders in the United States, 2001-2004, using data from the NAACCR and SEER programs. *Blood*. 2008;112(1):45–52. doi:10.1182/blood-2008-01-134858

3. Goldberg SL, Chen E, Corral M, et al. Incidence and clinical complications of myelodysplastic syndromes among United States Medicare beneficiaries. *J Clin Oncol*. 2010;28(17):2847–2852. doi:10.1200/JCO.2009.25.2395

4. Luskin MR, Lee JW, Fernandez HF, et al. Benefit of high-dose daunorubicin in AML induction extends across cytogenetic and molecular groups. *Blood*. 2016;127(12):1551–1558.

5. Voruganti S, Qin JJ, Sarkar S, et al. Oral nano-delivery of anticancer ginsenoside 25-OCH3-PPD, a natural inhibitor of the MDM2 oncogene: nanoparticle preparation, characterization, in vitro and in vivo anti-prostate cancer activity, and mechanisms of action. *Oncotarget*. 2015;6(25):21379–21394. doi:10.18632/oncotarget.4091

6. Gaur S, Wen Y, Song JH, et al. Chitosan nanoparticle-mediated delivery of miRNA-34a decreases prostate tumor growth in the bone and its expression induces non-canonical autophagy. *Oncotarget*. 2015;6 (30):29161–29177. doi:10.18632/oncotarget.v6i30

7. Fiorillo M, Verre AF, Iliut M, et al. Graphene oxide selectively targets cancer stem cells, across multiple tumor types: implications for non-toxic cancer treatment, via "differentiation-based nanotherapy". *Oncotarget*. 2015;6(6):3553–3562.

8. Basak SK, Zinabadi A, Wu AW, et al. Liposome encapsulated curcumin-difluorinated (CDF) inhibits the growth of cisplatin resistant head and neck cancer stem cells. *Oncotarget*. 2015;6 (21):18504–18517. doi:10.18632/oncotarget.v6i21

9. Yong KT, Law WC, Roy I, et al. Aqueous phase synthesis of CdTe quantum dots for biophotonics. *J Biophotonics*. 2011;4(1–2):9–20. doi:10.1002/jbio.201000080

10. Zhou Y, Wang R, Chen B, Sun D, Hu Y, Xu P. Daunorubicin and gambogic acid coloaded cysteamine-CdTe quantum dots minimizing the multidrug resistance of lymphoma in vitro and in vivo. *Int J Nanomedicine*. 2016;11:5429–5442. doi:10.2147/IJN

11. Peipei X, Zuo H, Chen D, et al. Anti-CD22-conjugated CdTe QDs co-loaded with doxorubicin and gambogic acid: a novel platform for lymphoma treatment. *RSC Adv*. 2017;7(54):33905–33913. doi:10.1039/C7RA04056C

12. Testa U, Riccioni R, Militi S, et al. Elevated expression of IL-3Ralpha in acute myelogenous leukemia is associated with enhanced blast proliferation, increased cellularity, and poor prognosis. *Blood*. 2002;100 (8):2980–2988. doi:10.1182/blood-2002-03-0852

13. Li LJ, Tao JL, Fu R, et al. Increased CD34+CD38-CD123 + cells in myelodysplastic syndrome displaying malignant features similar to those in AML. *Int J Hematol*. 2014;100(1):60–69. doi:10.1007/s12185-014-1590-2

14. Yue LZ, Fu R, Wang HQ, et al. Expression of CD123 and CD114 on the bone marrow cells of patients with myelodysplastic syndrome. *Chin Med J (Engl)*. 2010;123(15):2034–2037.

15. Gaponik N, Talapin DV, Rogach AL, et al. Thiol-capping of CdTe nanocrystals: an alternative to organometallic synthetic routes. *J Phys Chem B*. 2002;106(29):7177–7185. doi:10.1021/jp025541k

16. Wang S, Natalia Mamedova NA, Kotov W, Chen J. Studer, Antigen/antibody immunocomplex from CdTe nanoparticle bioconjugates. *Nano Lett*. 2002;2:817–822. doi:10.1021/nl0255193

17. Montalban-Bravo G, Garcia-Manero G. Myelodysplastic syndromes: 2018 update on diagnosis, risk-stratification and management. *Am J Hematol*. 2018;93(1):129–147. doi:10.1002/ajh.v93.1

18. Gordon MS. Advances in supportive care of myelodysplastic syndromes. *Semin Hematol*. 1999;36(4 Suppl 6):21–24.

19. Wattel E, De Botton S, Luc LJ, et al. Long-term follow-up of de novo myelodysplastic syndromes treated with intensive chemotherapy: incidence of long-term survivors and outcome of partial responders. *Br J Haematol*. 1997;98(4):983–991. doi:10.1046/j.1365-2141.1997.2973114.x

20. Olivares M, López MC, García-Pérez JL, Briones P, Pulgar M, Thomas MC. The endonuclease NL1Tc encoded by the LINE L1Tc from Trypanosoma cruzi protects parasites from daunorubicin DNA damage. *Biochim Biophys Acta*. 2003;1626(1–3):25–32. doi:10.1016/S0167-4781(03)00022-8

21. van Dalen EC, van der Pal HJ, Caron HN, Kremer LC. Different dosage schedules for reducing cardiotoxicity in cancer patients receiving anthracycline chemotherapy. *Cochrane Database Syst Rev*. 2009;4:CD005008.

22. Xie W, Wang X, Du W, Liu W, Qin X, Huang S. Detection of molecular targets on the surface of CD34+CD38-bone marrow cells in myelodysplastic syndromes. *Cytometry A*. 2010;77(9):840–848. doi:10.1002/cyto.a.20929

23. De Smet D, Trullemans F, Jochmans K, et al. Diagnostic potential of CD34+ cell antigen expression in myelodysplastic syndromes. *Am J Clin Pathol*. 2012;138(5):732–743. doi:10.1309/AJCPAGVO27RPTOTV

24. Shubayev VI, Pisanic TR, Jin S. Magnetic nanoparticles for theragnostics. *Adv Drug Deliv Rev*. 2009;61(6):467–477. doi:10.1016/j.addr.2009.03.007

25. Zaman S, Wang R, Gandhi V. Targeting the apoptosis pathway in hematologic malignancies. *Leuk Lymphoma*. 2014;55(9):1980–1992. doi:10.3109/10428194.2013.855307

26. Roos WP, Kaina B. DNA damage-induced cell death by apoptosis. *Trends Mol Med*. 2006;12(9):440–450. doi:10.1016/j.molmed.2006.07.007

27. Mohammadian J, Sabzichi M, Molavi O, Shanehbandi D, Samadi N. Combined treatment with static and docetaxel alters the Bax/Bcl-2 gene expression ratio in human prostate cancer cells. *Asian Pac J Cancer Prev*. 2016;17(11):5031–5035. doi:10.22034/APJCP.2016.17.11.5031

28. Xu P, Zuo H, Zhou R, et al. Doxorubicin-loaded platelets conjugated with anti-CD22 mAbs: a novel targeted delivery system for lymphoma treatment with cardiopulmonary avoidance. *Oncotarget*. 2017;8(35):58322–58337. doi:10.18632/oncotarget.16871